

Understanding the graphitization and growth of free-standing nanocrystalline graphene using *in situ* transmission electron microscopy†

C. N. Shyam Kumar,^{a,b} Venkata Sai Kiran Chakravadhanula,^{b,c} Adnan Riaz,^{a,b} Simone Dehm,^a Di Wang,^{a,d} Xiaoke Mu,^a Benjamin Flavel,^a Ralph Krupke^{a,b} and Christian Kübel^{a,c,d}

Graphitization of polymers is an effective way to synthesize nanocrystalline graphene on different substrates with tunable shape, thickness and properties. The catalyst free synthesis results in crystallite sizes on the order of a few nanometers, significantly smaller than commonly prepared polycrystalline graphene. Even though this method provides the flexibility of graphitizing polymer films on different substrates, substrate free graphitization of freestanding polymer layers has not been studied yet. We report for the first time the thermally induced graphitization and domain growth of free-standing nanocrystalline graphene thin films using *in situ* TEM techniques. High resolution transmission electron microscopy (HRTEM), selected area electron diffraction (SAED) and electron energy loss spectroscopy (EELS) techniques were used to analyze the graphitization and the evolution of nanocrystalline domains at different temperatures by characterizing the crystallinity and domain size, further supported by *ex situ* Raman spectroscopy. The graphitization was comparable to the substrate supported heating and the temperature dependence of graphitization was analyzed. In addition, the *in situ* analysis of the graphitization enabled direct imaging of some of the growth processes taking place at different temperatures.

Introduction

Graphene, the sp^2 -hybridized single atomic layer of carbon, and closely related graphenoid materials have emerged as candidates for future technological applications in a wide variety of fields due to their unique properties.¹ Because of their

structure and low dimensionality, the mechanical and electrical behavior of these two-dimensional materials differs considerably from bulk graphite. The properties of graphene largely depend on the thickness, edge morphology and defect structure.² Different methods have been used to successfully produce large-area graphene for a variety of applications.³ These commonly used methods need a catalytic surface for the growth of graphene films with an additional transfer process onto different substrates for most of the practical purposes. This may induce defects and contamination affecting the inherent properties of the material.

Recent advances in the catalyst-free synthesis of graphene enable the production of graphene materials on different substrates with a controllable shape and thickness by thermal graphitization of thin polymer films.^{4–6} These materials are termed graphenoid (graphene like) materials and the technological importance of these materials is increasing in areas such as electronics,^{4,5} photonics,^{6,7} strain sensing,⁶ or transparent conducting electrodes^{8,9} to mention just a few. This catalyst-free growth results in domain sizes on the order of a few nanometers and can be termed nanocrystalline graphene. It provides the flexibility of growing on different substrates with a defined thickness and also for patterning to achieve different shapes.⁶ This bottom up approach also provides control to tailor the properties of the final structure by varying the graphitization conditions, which determine the crystallinity and domain size. Despite the growing acceptance of these materials in different fields, the dynamics of graphitization and domain growth is still poorly understood. Since the properties of these graphitized carbon structures are largely affected by the domain size and other defects, a detailed understanding of the graphitization and domain growth as a function of temperature is essential for controlled tailoring of the properties of the graphitic material.

For the preparation of nanocrystalline graphene, different source materials and processes are used for the initial polymer film, which is then graphitized by substrate supported vacuum annealing. The flexibility of graphitizing these polymer films

^aInstitute of Nanotechnology, Karlsruhe Institute of Technology, 76021 Karlsruhe, Germany. E mail: christian.kuebel@kit.edu

^bDepartment of Materials and Earth Sciences, Technische Universität Darmstadt, 64287 Darmstadt, Germany

^cHelmholtz Institute Ulm, 89081 Ulm, Germany

^dKarlsruhe Nano Micro Facility, Karlsruhe Institute of Technology, 76021 Karlsruhe, Germany

†Electronic supplementary information (ESI) available. See DOI: 10.1039/c7nr03276e

on different substrates has been demonstrated.^{4–6} Substrate free graphitization of free-standing polymer films has not been reported yet. There are only some reports on the graphitization of suspended carbon nanowires.^{10,11} Considering the technological importance of free-standing graphene films,^{12,13} these free-standing nanocrystalline graphene films with tunable shape, thickness and properties will be an interesting candidate for electronic and optoelectronic applications.

High resolution transmission electron microscopy (HRTEM) is an effective tool for the structural characterization of carbon nanostructures with sub-angstrom resolution.^{14,15} Low voltage HRTEM facilitates the characterization of graphene related materials without inducing significant beam damage or defects.^{16,17} Recent advances in *in situ* HRTEM enabled the analysis of different structural changes during *in situ* heating,^{18–20} electrical biasing^{21,22} of graphene and *in situ* heating of other carbon nanostructures.^{23–25} Here we report on the graphitization and domain growth of free-standing nanocrystalline graphene thin films prepared by vacuum annealing of a photoresist inside a TEM and following the process by *in situ* TEM techniques. HRTEM, selected area electron diffraction (SAED) and electron energy loss spectroscopy (EELS) techniques were used to analyze the graphitization and the evolution of nanocrystalline domains at different temperatures. This is the first attempt to grow free-standing nanocrystalline graphene by the graphitization of a polymer thin film inside a TEM and to follow the growth by *in situ* TEM techniques. The *in situ* process eliminates possible artefacts associated with the transfer process shadowing the true structural transformations. The *in situ* growth results in large freestanding thin membranes, which can be analyzed in depth for precise information about the structural changes during graphitization and domain growth. The use of pre-calibrated, MEMS based heating chips enables a good correlation of the temperature and the corresponding structural changes.

Experimental procedure

The photoresist used as the carbon source for the nanocrystalline graphene preparation is the commercially available photoresist, microposit S1805. The photoresist was diluted with propylene glycol monomethyl ether acetate (PGMEA) by 1 : 12 to tune the viscosity and resulting film thickness. The resist was spin coated onto a MEM based heating chip (Protochips Inc.) at 8000 rpm for 30 seconds and then baked at 160 °C for 3 minutes resulting in a thin film covering the whole heating chip.

The active part of the heating chip consists of a free-standing ceramic membrane coated with a thin amorphous SiN film with patterned holes acting as the sample support and the ceramic as the heating element.²⁶ The electrodes of the heating chip were exposed by dipping it into acetone (Fig. 1). The chip was loaded into a heating holder (Aduro 500 by Protochips Inc.). The initial heating was carried out inside a Gatan pumping station at 10^{-7} mbar at a temperature of

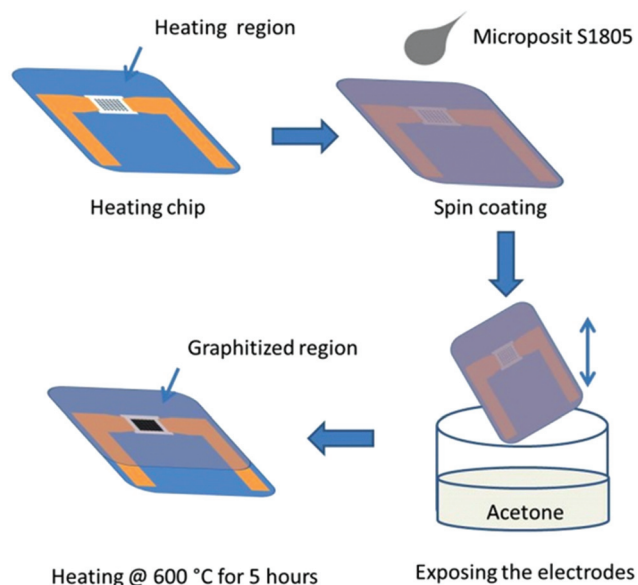


Fig. 1 Schematic process flow of the graphitization on a MEMS heating device. The chip was spin coated with the photoresist and the electrodes were exposed by dipping in acetone.

600 °C for 5 hours (heating rate 10 °C per minute) to prevent the contamination of the TEM by the large amount of gas released during the initial stages of graphitization.

The graphitized samples were characterized using confocal Raman spectroscopy and TEM. Raman spectroscopy was carried out with a Renishaw Raman microscope with 514 nm laser excitation. The Raman map was acquired from a $13 \mu\text{m} \times 2 \mu\text{m}$ area with a step size of $1 \mu\text{m}$. The peak intensities and the intensity ratio map were obtained using the WiRE software (Renishaw Raman software). An aberration corrected (image) Titan 80-300 TEM (FEI Company) operated at 80 kV equipped with a Tridium 863 imaging filter (Gatan Inc.) was used for EEL spectroscopy and a US1000 slowscan CCD (Gatan Inc.) was used for imaging and diffraction. All EEL spectra were acquired in STEM mode with a convergence angle of 1.5 mrad and an acceptance angle of 4 mrad. These experimental conditions satisfy the magic angle condition at 80 kV to eliminate the dependence of π^* and σ^* intensities on the orientation of the isotropic graphene structures with respect to the incident beam.^{27,28} Five spectra from different places were acquired at each temperature to evaluate the sp^2 content during the graphitization of the polymer. The *in situ* heating experiments were carried out starting at 600 °C since the samples were already *ex situ* graphitized at 600 °C for 5 hours. A heating rate of 10 °C per minute was always used. The samples were heated inside the TEM to 600 °C with the beam blanked to prevent beam induced transformations. Bright field TEM images and SAED patterns were acquired at 100 °C intervals after holding the temperature for 10 minutes to ensure stable imaging conditions. For the diffraction analysis, a nominally parallel beam setting was used and the diffraction pattern was focused accurately. Intensity profiles of the SAED patterns were extracted

and analyzed using PASAD.²⁹ The beam was blanked after imaging to minimize the exposure. Also the images from the non-exposed areas were compared at each temperature to analyze the beam induced effect on the graphitization. During the reheating experiment, images were obtained every 10 °C and the structure is compared with non-exposed areas at each temperature.

Results and discussion

Graphitization of the free-standing layer on the MEMS device

Fig. 2 shows the optical and Raman characterization of the annealed photoresist on the heating chip after *ex situ* graphitization at 600 °C. Free-standing films have formed across the 5 micron diameter holes. The graphitic character of the free-standing film is comparable to that of the substrate supported film (Fig. 2b) as analyzed by Raman spectroscopy. The Raman signature (peak positions and I_D/I_G ratio) is almost identical to the *ex situ* graphitization on the SiO₂ terminated Si wafer. The spectrum consists of the G peak at around 1600 cm⁻¹, the D peak at around 1300 cm⁻¹ and a broad 2D and D + G region around 2800 cm⁻¹, which is characteristic of a partially graphitized material. Considering the peak position and I_D/I_G ratio and comparing it with the materials proposed in the graphitization trajectory by Ferrari *et al.*,³⁰ we can conclude that the material is nanocrystalline with some amount of sp³ coordinated amorphous carbon left. This is expected since the graphitization temperature is fairly low and does not facilitate complete graphitization. Fig. 2(c) shows the position of the G peak across the active heating area of the chip after heating to 600 °C. It reveals a homogeneous graphitized film across the active part of the chip. Fig. 2(d) shows a high resolution Raman map (I_D/I_G ratio) overlaid on the top of an optical image of the free-standing film across a hole. The color bar

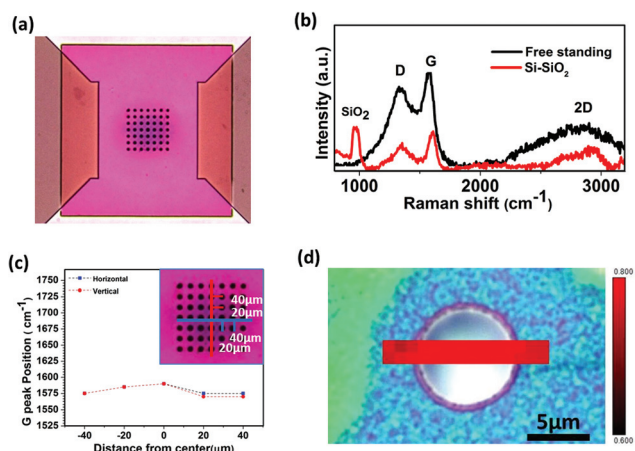


Fig. 2 (a) Optical micrograph of the graphitized heating area, (b) Raman spectra of the film graphitized at 600 °C, (c) G peak position near the center hole on the heating chip, (d) I_D/I_G ratio map overlaid on an optical image of a free standing film over a hole on the heating chip, the color scale shows the variation in the I_D/I_G ratio.

gives the variation of the I_D/I_G ratio across the free standing and the substrate supported area. It can be clearly observed from the map that the intensity ratio variation is negligible. This confirms that the graphitization is uniform over the free-standing layer. The I_D/I_G ratio outside the hole is slightly lower than that for the free-standing film, probably because of the Si/SiN support contributing to the background of the Raman spectrum in the supported region.

This analysis clearly shows that after *ex situ* heating to 600 °C for 5 h, free-standing graphitized films have formed across the holes of the supporting film on the heating chip. This confirms that free-standing polymer films were formed during the spin coating and a substrate free graphitization is possible. While it is well known that the source photoresist S1805 contains aromatic molecules, which can be graphitized at higher temperatures on a substrate, this confirms that graphitization without any catalytic support from the substrate is possible and yields very similar materials.

From previous studies on different substrates, it is known that the graphitization process starts at around 600 °C and yields increasingly graphitized nanocrystalline domains at least up to 1000 °C.⁵⁻⁷ This structural evolution was studied in the following *in situ* study under a TEM.

In situ heating

In situ TEM observations were made on the free-standing graphitized films from 600 °C to 1200 °C. The thin free-standing films were ideal for TEM observation to obtain detailed insights into the structural changes during heating. Fig. 3(a-g) show a series of bright field-TEM (BF-TEM) images of the growth of nanocrystalline domains during heating at increasing temperature. The evolution of the nanocrystalline domains with temperature can be observed in the images. At 600 °C, the structure is dominated by curved and wrinkled small features. It is well known that, during the graphitization of a polymer precursor, after the initial carbonization, the material consists of small domains of hexagonally coordinated aromatic molecules extending up to a few nanometers in size.³¹ The space between these crystallites is filled with disordered carbon or voids. As the temperature increases, increasing ordering of the crystallites occurs and the crystallite sizes increase by consuming the disordered carbon around it.³² This can be seen from the images at intermediate temperatures (600 °C to 1000 °C). At 800 °C, defined domains are visible in the BF-TEM images with an estimated size of 2–4 nm. At 1000 °C, the crystallites are more defined and subsequent heating results in an increase of the domain and crystallite size by merging of small crystallites to form bigger ones. This can be seen from Fig. S1† which shows merging of domains during heating from 1100 °C to 1200 °C. The structures observed at different temperatures *in situ* are compared with the previously unexposed areas at the same temperature and as they look very similar, beam damage effects do not significantly alter the observed graphitization process.

The evolution of the crystallite size was determined from SAED intensity profiles (Fig. 4a) using a simple Scherrer ana-

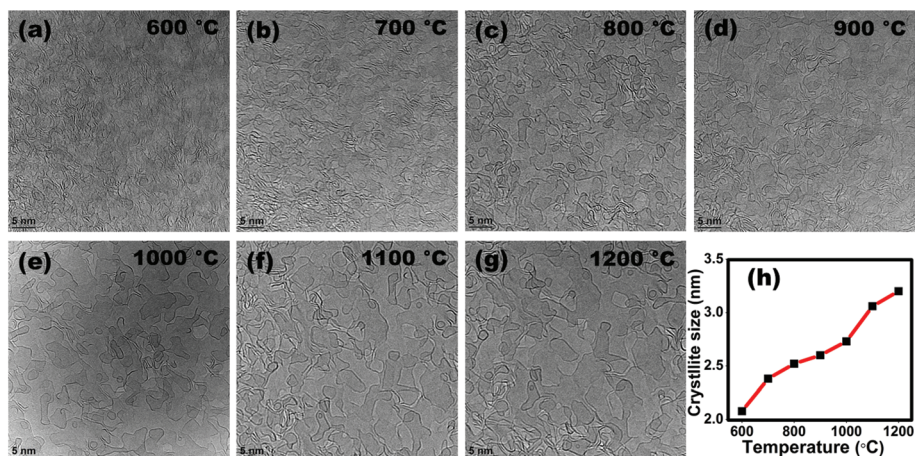


Fig. 3 (a-g) Growth of nanocrystalline domains and (h) crystallite size with increasing temperature.

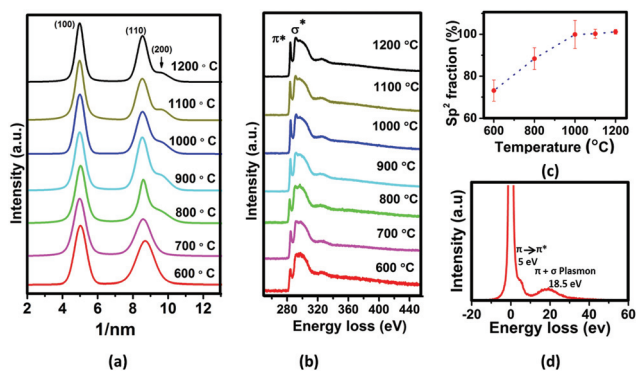


Fig. 4 (a) SAED intensity profile and (b) EELS carbon core loss spectra at different temperatures; (c) sp^2 content at different temperatures and (d) low loss region of the freestanding layer at 1200 °C.

lysis of the $\{100\}$ diffraction rings.³³ Experimental beam broadening was not subtracted for the Scherrer analysis, but the contribution is negligible for these small grain sizes. The average crystallite size increased from 2 nm at 600 °C to 3.2 nm at 1200 °C. The domain size determined at 1200 °C from BF-TEM images (6–8 nm) is greater than the crystallite size obtained from the Scherrer analysis. The difference is because by electron diffraction we measure the coherent scattering size, whereas the BF-TEM images are not very sensitive to small-angle boundaries and individual defects. The SAED determined crystallite size at 1000 °C (2.7 nm) is comparable to the previous reports on *ex situ* graphitization on different substrates.^{6,34} This confirms that the temperature dependence of graphitization in free-standing films is comparable to the substrate supported graphitization. Indexing the diffraction rings at different temperatures shows that the growth of graphene is in plane with a strong $[001]$ texture, whereas there is no indication of a $\{002\}$ peak at around 2.9 nm^{-1} (Fig. 4a). As the temperature increases, the width of diffraction rings reduces and a weak diffraction ring corresponding to (200) starts to evolve at 800 °C. This is in agreement with the TEM obser-

vation that the domains become more ordered at 800 °C. At higher temperatures, the width of the diffraction peaks decreases and the (200) peak becomes more defined confirming the growth of the crystallites as plotted in Fig. 3h and an increasing order.

Fig. 4b shows the EELS data of the carbon core-loss edge at different temperatures during heating. At 600 °C, the core loss edge of carbon resembles an amorphous structure containing a low-intensity π^* peak at 285 eV followed by a featureless σ^* and extended near edge region. The peak near 285 eV corresponds to the transition from the $1s$ to π^* orbital and is a characteristic feature of sp^2 bonding. This means that at 600 °C the material is amorphous in nature with considerable amounts of sp^2 and sp^3 bonding.³⁵ As the temperature increases, the intensity of the π^* transition increases indicating an increase in sp^2 character. In addition, the σ^* and ELNES region becomes increasingly structured indicating an increased graphitic order.^{36,37} There is also an increase in the intensity of the multiple scattering resonance (MSR) peak around 330 eV with increasing temperature.³⁸ This evolution can be attributed to the decreasing variation in the nearest neighbor and next nearest neighbor atomic distance and reflects the formation of well-defined coordination spheres. The sp^2 content of the graphitized layer at different temperatures is measured from the core loss spectra. The integrated intensity ratio of the π^* over the $\pi^* + \sigma^*$ transition was compared with a fully graphitized standard.³⁹ The integrated intensity of the π^* peak is calculated using a 5 eV window from the onset of the peak at 282.5 eV and the $\pi^* + \sigma^*$ integrated intensity is calculated using a 50 eV window starting from the same region. The standard deviation of the sp^2 content of the 5 individual measurements at each temperature is used to estimate the measurement error. Fig. 4(c) shows the evolution of the sp^2 content with temperature. It increases from 600 °C to 1000 °C and then saturates. This confirms that the material is completely graphitized around 1000 °C and further growth is facilitated by the merging of graphene domains. We compared the sp^2 content determined by EELS with the Raman spectra

recorded for a sample heated at 1200 °C (Fig. S2†). The spectra at 1200 °C consist of well-defined D, G, 2D and D + G peaks indicating an increased graphitic character compared to the amorphous film heated to 600 °C. The presence of the D peak is characteristic of the nanocrystalline nature of the film.^{4,5} The D peak is a disorder induced peak in sp^2 carbon, which can occur due to defects and/or small crystallite sizes and would be absent for defect free completely graphitized samples. The I_D/I_G ratio and the position of the G peak can be used to analyze the percentage of sp^2 bonding and the defect density. Comparing the I_D/I_G ratio (1.26) and G peak position (1585 cm^{-1}) with the graphitization trajectory proposed by Ferrari *et al.*,³⁰ the Raman spectra at 1200 °C fit well to nanocrystalline graphite with 100% sp^2 content as discussed in previous work.⁶ This confirms that the sample is fully graphitic in nature in agreement with the EELS analysis.

Fig. 4d shows the low-loss peak in a region around 1.5 microns away from the edge of the free standing graphitized layer at 1200 °C. The low loss shows two distinct peaks around 5 eV and 18.5 eV. The first peak corresponds to the $\pi-\pi^*$ inter-band transition and the second one is due to the collective oscillation of the $\pi + \sigma$ plasmon. The $\pi-\pi^*$ transition is mainly due to the in-plane mode, which appears at 7 eV for graphite and shifts to 4.8 eV for single layer graphene. The $\pi + \sigma$ plasmon peak also exhibits a red-shift from 27 eV for graphite to 15 eV for graphene.⁴⁰ From the core loss and low loss spectra at 1200 °C, we can conclude that the structure consists of a few layers of highly graphitic nanocrystalline material. However, further away from the edge, we also observed some thicker graphitic areas.

HRTEM images of the graphitized layer obtained immediately after cooling from 1200 °C are shown in Fig. 5a and b. The formation of extended graphene domains stacked on top of each other is evident from the images. Apart from the large domains, we can also see some small graphitic structures with sizes of 2 nm or less (marked by white arrows). These small structures probably remained from the earlier stages of the domain growth. Some of them are quite mobile on the surface of larger graphene domains and will combine to form bigger domains when heated further. Fig. 5c and d show the coalescence of two small structures forming one during the heating process. During the merging, the shape of the small structure is changing; this can also be observed in the small structures adjacent to the merging structures. This shows that the movement of the domains is not coherent rather facilitated by the movement of individual atoms or a group of atoms. It should also be noted that the larger domains may contain defects that presumably form during merging of smaller domains (marked by red arrows). FFTs from two different regions marked in Fig. 5a are given in the inset. The first FFT shows six reflections corresponding to a single crystalline region and the adjacent region contains another set of spots rotated by 22° . This corresponds to a few layers of graphene misoriented by 22° . The same misorientation angle is also observed in the marked region also in Fig. 5b. This misorientation angle (21.79°) is commonly observed in multilayer graphene, corresponding to

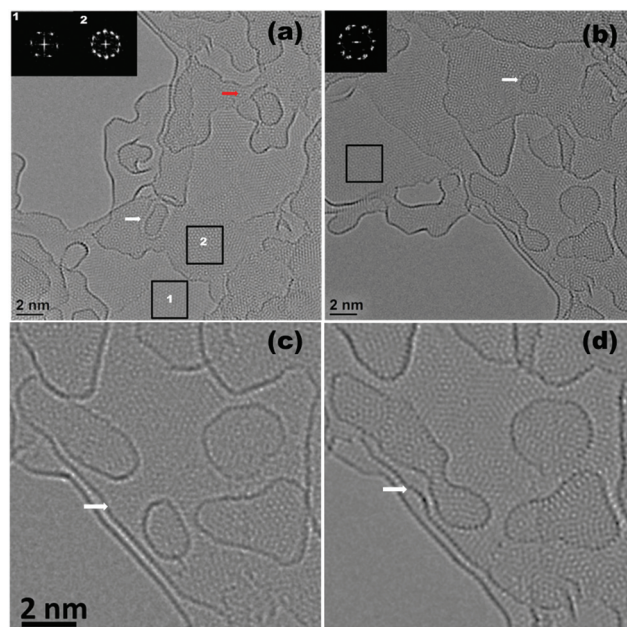


Fig. 5 (a, b) HRTEM images of an edge heated to 1200 °C; (c) and (d) merging of two small graphitic structures by coalescence during heating at 1200 °C.

a low energy commensurate structure.^{41–43} It has been reported during the catalyst free transformation of amorphous carbon on the top of a graphene substrate.⁴⁴ Furthermore, we can see that the edges of the layers do not exhibit well-defined facets. This means that the edges may also contain unsaturated bonds and/or pentagon–heptagon rings.^{19,45} Nevertheless, we also observed a transformation to better defined facets after prolonged heating (Fig. S3†).

Reheating of graphitized layers

We observed a significant amount of carbonaceous material on the graphitized samples after exposing the samples to the atmosphere and reinserting them into the TEM (Fig. S4b†). As can be observed from the high resolution images in Fig. 5, the graphitized layers contain lots of free edges and surface, favorable for adsorption of the carbonaceous material. Heating the sample with these amorphous deposits can yield additional information on the formation and growth of the domains. A structure consisting of domains with active edges surrounded by amorphous carbon is similar to the structure during the early stages of graphitization. Thus, we believe that the structural changes during heating of the sample with the carbonaceous material can be correlated with the early stages of the graphitization and growth of the nanocrystalline domains.

Samples with additional amorphous impurities from air exposure on the surface were heated inside the microscope and the changes in the amorphous and crystalline regions were studied (Fig. S4†). We observed two main transformations in the amorphous region. (1) Amorphous regions near and/or attached to domain edges crystallize and become attached at

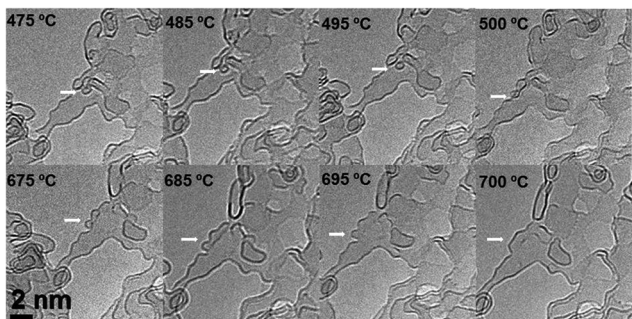


Fig. 6 Migration and merging of a small graphitic domains.

the edge of the domain, increasing the size of the domain. (2) Graphitization of amorphous carbon formed small graphitic structures on top of the graphitized layers. These newly formed small graphitic structures are mobile and can get attached/merge with the edges of neighboring domains (Fig. S5†). The size distribution of these small graphitic structures is broad, varying in shape and size up to 5 nm. Some of the observed structures have sizes comparable to fullerenes and could be a cage like structure.^{46,47} Fig. 6 shows the movement and attachment of a small graphitic structure (size less than 1 nm) to the edge of a layer during heating. This structure was formed during the re-heating. At intermediate temperatures (475 °C to 500 °C), it becomes detached from a minor edge, moves on the surface towards the edge of a larger domain, and becomes attached to the new edge. As the temperature increases (675 °C to 700 °C), both graphitic structures merge at the edge of the layer, extending the graphene sheet. High resolution images from this region (Fig. S5†) confirm that the small structure completely merged with the layer without noticeable discontinuity. Considering the previous reports on the formation and high mobility of fullerene like structures on glassy carbon and on the top of graphene,^{48,49} these could be the bend graphitic structures formed by transformation of amorphous deposits. In addition, there are also a significant number of trapped structures, which have been formed during the initial heating and are stable even after the reheating cycle (Fig. S6†), suggesting that different structures with very different properties form during the heating.

Discussion

Graphitization of carbons from different sources is a well-studied field. Different models were proposed for the graphitization and crystallite growth during heating from different source materials.^{31,32,50} According to the proposed models, at intermediate temperatures, after the initial carbonization of the polymer, the structure consists of small misoriented crystallites with the space between them filled by uncoordinated amorphous carbon or voids. These small crystallites contain 3 to 4 layers of hexagonally coordinated aromatic molecules with sizes extending up to a couple of nanometers. The graphitiz-

ability of these structure depends on their misorientation and the void size between the crystallites.^{31,32,50,51} It is seen from the TEM images that the structure at 600 °C consists of small misoriented crystallites. From 600 °C to 800 °C, the domains transform into a more extended and ordered structure. The amorphous carbon around the domains is consumed in this process. This transformation and growth is visible looking at the decreasing width of the (100) peak in SAED and the appearance of the (200) peak as well as from the increase of the sp^2 content, evident from the EEL spectra. This growth continues until the sample is almost completely graphitized around 1000 °C. Further growth of the crystalline domains is facilitated by coalescence of the small crystallites above 1000 °C. In our experiments the layer formation was imaged for a completely free-standing film, while the structure of the final graphitized film is comparable to the graphitization of substrate supported films. This is evident from the comparable average crystallite size and sp^2 content of the film grown on different substrates. This opens up new possibilities to learn more about the inherent processes during the graphitization of polymer precursors excluding the substrate effects. Comparable graphitization of these free-standing films can also provide new methods for the fabrication of freestanding graphitic films with tunable shape and properties.

The reheating experiments after exposure to air provide a suitable environment for analyzing the mechanisms operating during the initial stages of graphitization. The attachment of the carbonaceous materials at the edges can be explained by the fact that disordered and active edges facilitate the attachment of amorphous carbon. Formation of new graphitic nuclei from the amorphous adsorbates occurs by catalyst free transformation of the carbon species on top of graphene. *In situ* TEM experiments with current induced annealing by Barreiro *et al.*⁴⁴ showed the transformation of absorbed amorphous carbon on a graphene substrate, transforming into graphene sheets. The experiment and molecular dynamic simulation showed that the amorphous carbon on top of graphene will not sublime but rather transform to small graphene flakes, which further combine to form large area graphene at elevated temperatures. The newly formed layers exhibited a misorientation of 22°, which was also observed in the present study. A similar transformation was also reported by Westenfelder *et al.*,⁵² where the amorphous carbon was converted into polycrystalline layers of graphene. From the HRTEM images and the corresponding FFT we believe that in the present study similar transformations were operating converting amorphous carbon to graphene. The small, flat, well distributed graphitic structures originate from these kinds of transformations. The formation of structures with size of less than 1 nm and fullerene like appearance is yet to be fully understood. One possible mechanism could be bending and conversion of the small flat graphitic structure formed from the amorphous carbon to a caged structure on the top of graphene as observed by Chuvilin *et al.*⁵³ This transformation has been reported to happen under the influence of the electron beam, which results in knock on damage at the edges, leading to the for-

mation of pentagons and thus subsequent bending. Neng *et al.*⁵⁴ also observed the transformation of small graphene flakes into fullerene by the addition of atom by atom through an add-atom mechanism from the graphene edge. Adding atoms at the edge results in the formation of pentagon and heptagon rings which induces the bending and formation of the cage structure. This transformation was also reported under the influence of an electron beam. In our case, similar structures are observed in previously unexposed areas, which means that these structures are not formed because of beam damage. However, the addition of atoms and the formation of pentagons/heptagon could also happen without the electron beam at the edges of these small graphitic structures when they are continuously growing. This could trigger the bending and closure of the edges as heating may provide the favorable condition.

The difference in the mobility of these small structures is also an interesting observation. Cage-like structures would be expected to be more mobile on top of the graphitic substrates due to their weaker interactions with the substrate compared to extended planar graphitic structures. Therefore, the observation of both mobile structures and trapped structures, which do not move even after two heating cycles, could be an indication of the presence of the planar and cage-like structure. However, with the substrate structure being far from perfectly crystalline, there are a considerable number of defect sites (sp^3 centers, voids, grain boundaries) which could also pin the motion of small graphitic structures and explain the immobile graphitic structures. The size and the shape of these trapped structures are changing during heating. The size of the trapped structures reduced after the reheating. This reduction in size is also observed during prolonged heating (Fig. S3†). This suggests that individual atoms or group of atoms can detach and move from the small graphitic structures, probably corresponding to Ostwald ripening.

Conclusion

We performed *in situ* TEM studies to understand the graphitization and grain growth in nanocrystalline graphene during heating of a free-standing polymer film. The graphitization of the free-standing film was comparable to substrate supported graphitization. However, in our *in situ* observations, we directly imaged the details of the growth processes. The growth of the crystallites in the intermediate temperature range of 600–1000 °C mainly occurs by consuming residual amorphous carbon around graphitic domains. The amorphous carbon transforms in one of two ways, either by attaching to the active edges of graphitic domains or by catalyst free growth on top of a graphitic layer. This catalyst free transformation forms new small graphitic structures, some of which are highly mobile at higher temperatures and get attached to the edges, extending the edges. At higher temperatures of 1000–1200 °C, larger domains become mobile and the growth proceeds by merging of these mobile domains on the surface of preformed graphene layers.

Acknowledgements

CNSK greatly acknowledges the PhD funding from the Deutscher Akademischer Austauschdienst (DAAD). BSF gratefully acknowledges the support from the Deutsche Forschungsgemeinschaft (DFG) under grant numbers FL 834/1-1 and FL 834/2-1. RK acknowledges funding by the DFG under INST 163/354-1 FUGG.

References

- 1 K. S. Novoselov, V. I. Fal, L. Colombo, P. R. Gellert, M. G. Schwab and K. Kim, *Nature*, 2012, **490**, 192–200.
- 2 L. Liu, M. Qing, Y. Wang and S. Chen, *J. Mater. Sci. Technol.*, 2015, **31**, 599–606.
- 3 R. S. Edwards and K. S. Coleman, *Nanoscale*, 2013, **5**, 38–51.
- 4 Z. Zhang, B. Ge, Y. Guo, D. Tang, X. Wang and F. Wang, *Chem. Commun.*, 2013, **49**, 2789–2791.
- 5 A. Turchanin, D. Weber, M. Büenfeld, C. Kisielowski, M. V. Fistul, K. B. Efetov, T. Weimann, R. Stosch, J. Mayer and A. Götzhäuser, *ACS Nano*, 2011, **5**, 3896–3904.
- 6 A. Riaz, F. Pyatkov, A. Alam, S. Dehm, A. Felten, V. S. K. Chakravadhanula, B. S. Flavel, C. Kübel, U. Lemmer and R. Krupke, *Nanotechnology*, 2015, **26**, 325202.
- 7 Z. Zhang, Y. Guo, X. Wang, D. Li, F. Wang and S. Xie, *Adv. Funct. Mater.*, 2014, **24**, 835–840.
- 8 S.-Y. Son, Y.-J. Noh, C. Bok, S. Lee, B. G. Kim, S.-I. Na and H.-I. Joh, *Nanoscale*, 2014, **6**, 678–682.
- 9 H. Medina, Y. C. Lin, C. Jin, C. C. Lu, C. H. Yeh, K. P. Huang, K. Suenaga, J. Robertson and P. W. Chiu, *Adv. Funct. Mater.*, 2012, **22**, 2123–2128.
- 10 S. Sharma, A. Sharma, Y. K. Cho and M. Madou, *ACS Appl. Mater. Interfaces*, 2012, **4**, 34–39.
- 11 T. Maitra, S. Sharma, A. Srivastava, Y. K. Cho, M. Madou and A. Sharma, *Carbon*, 2012, **50**, 1753–1761.
- 12 I. K. Moon, B. Ki, S. Yoon, J. Choi and J. Oh, *Sci. Rep.*, 2016, **6**, 33525.
- 13 H. Wei, S. Wei, W. Tian, D. Zhu, Y. Liu, L. Yuan and X. Li, *Sci. Rep.*, 2014, **4**, 28–31.
- 14 J. A. Rodríguez-Manzo, A. V. Krasheninnikov and F. Banhart, *ChemPhysChem*, 2012, **13**, 2596–2600.
- 15 F. Banhart, J. Kotakoski and A. V. Krasheninnikov, *ACS Nano*, 2011, **5**, 26–41.
- 16 A. W. Robertson, G.-D. Lee, K. He, E. Yoon, A. I. Kirkland and J. H. Warner, *Nano Lett.*, 2014, **14**, 1634–1642.
- 17 O. Lehtinen, I.-L. Tsai, R. Jalil, R. R. Nair, J. Keinonen, U. Kaiser and I. V. Grigorieva, *Nanoscale*, 2014, **6**, 6569–6576.
- 18 N. Lu, J. Wang, H. C. Floresca and M. J. Kim, *Carbon*, 2012, **50**, 2961–2965.
- 19 K. He, A. W. Robertson, Y. Fan, C. S. Allen, Y. Lin, K. Suenaga, A. I. Kirkland and J. H. Warner, *ACS Nano*, 2015, **9**, 4786–4795.
- 20 Z. Liu, Y.-C. Lin, C.-C. Lu, C.-H. Yeh, P.-W. Chiu, S. Iijima and K. Suenaga, *Nat. Commun.*, 2014, **5**, 1–7.

- 21 Z. J. Qi, J. A. Rodríguez-Manzo, A. R. Botello-Méndez, S. J. Hong, E. A. Stach, Y. W. Park, J. Charlier, M. Drndić and A. T. C. Johnson, *Nano Lett.*, 2014, **14**, 4238–4244.
- 22 Q. Wang, R. Kitaura, S. Suzuki, Y. Miyauchi, K. Matsuda, Y. Yamamoto, S. Arai and H. Shinohara, *ACS Nano*, 2016, **10**, 1475–1480.
- 23 H. Yoshida, S. Takeda, T. Uchiyama, H. Kohno and Y. Homma, *Nano Lett.*, 2008, **8**, 2082–2086.
- 24 R. Sharma and Z. Iqbal, *Appl. Phys. Lett.*, 2004, **84**, 990–992.
- 25 L. Fei, T. Sun, W. Lu, X. An, Z. Hu, J. C. Yu, R. Zheng, X. Li, H. L. W. Chan and Y. Wang, *Chem. Commun.*, 2014, **50**, 826–828.
- 26 L. F. Allard, W. C. Bigelow, M. Jose-Yacamán, D. P. Nackashi, J. Damiano and S. E. Mick, *Microsc. Res. Tech.*, 2009, **72**, 208–215.
- 27 H. Daniels, A. Brown, A. Scott, T. Nichells, B. Rand and R. Brydson, *Ultramicroscopy*, 2003, **96**, 523–534.
- 28 C. Hébert, P. Schattschneider, H. Franco and B. Jouffrey, *Ultramicroscopy*, 2006, **106**, 1139–1143.
- 29 C. Gammer, C. Mangler, C. Rentenberger and H. P. Karnthaler, *Scr. Mater.*, 2010, **63**, 312–315.
- 30 A. C. Ferrari and J. Robertson, *Philos. Trans. R. Soc. London, Ser. A*, 2004, **362**, 2477–2512.
- 31 P. J. F. Harris, *Crit. Rev. Solid State Mater. Sci.*, 2005, **30**, 235–253.
- 32 R. E. Franklin, *Proc. R. Soc. London, Ser. A*, 1951, **209**, 196–218.
- 33 C. Oprea, V. Ciupina and G. Prodan, *Rom. Rep. Phys.*, 2008, **53**, 223–230.
- 34 P. Angelova, H. Vieker, N. E. Weber, D. Matei, O. Reimer, I. Meier, S. Kurasch, J. Biskupek, D. Lorbach, K. Wunderlich, L. Chen, A. Terfort, M. Klapper, K. Müllen, U. Kaiser, A. Götzhäuser and A. Turchanin, *ACS Nano*, 2013, **7**, 6489–6497.
- 35 P. K. Chu and L. Li, *Mater. Chem. Phys.*, 2006, **96**, 253–277.
- 36 R. A. Rosenberg, P. J. Love and V. Rehn, *Phys. Rev. B: Condens. Matter*, 1986, **33**, 4034–4037.
- 37 A. C. Ferrari, A. Libassi, B. K. Tanner, V. Stolojan, J. Yuan, L. M. Brown, S. E. Rodil, B. Kleinsorge and J. Robertson, *Phys. Rev. B: Condens. Matter*, 2000, **62**, 11089–11103.
- 38 H. Daniels, R. Brydson, B. Rand and A. Brown, *Philos. Mag.*, 2007, **87**, 4073–4092.
- 39 S. D. Berger, D. R. McKenzie and P. J. Martin, *Philos. Mag. Lett.*, 1988, **57**, 285–290.
- 40 T. Eberlein, U. Bangert, R. R. Nair, R. Jones, M. Gass, A. L. Bleloch, K. S. Novoselov, A. Geim and P. R. Briddon, *Phys. Rev. B: Condens. Matter Mater. Phys.*, 2008, **77**, 1–4.
- 41 J. M. Campanera, G. Savini, I. Suarez-Martinez and M. I. Heggie, *Phys. Rev. B: Condens. Matter*, 2007, **75**, 235449.
- 42 E. Cisternas, M. Flores and P. Vargas, *Phys. Rev. B: Condens. Matter*, 2008, **78**, 125406.
- 43 T. G. Mendes-de-Sa, A. M. B. Goncalves, M. J. S. Matos, P. M. Coelho, R. Magalhaes-Paniago and R. G. Lacerda, *Nanotechnology*, 2012, **23**, 475602.
- 44 A. Barreiro, F. Börrnert, S. M. Avdoshenko, B. Rellinghaus, G. Cuniberti, M. H. Rummeli and L. M. K. Vandersypen, *Sci. Rep.*, 2013, **3**, 1115.
- 45 P. Koskinen, S. Malola and H. Häkkinen, *Phys. Rev. B: Condens. Matter*, 2009, **80**, 073401.
- 46 T. Uwanno, Y. Hattori, T. Taniguchi, K. Watanabe and K. Nagashio, *2D Mater.*, 2015, **2**, 041002.
- 47 T. Füller and F. Banhart, *Chem. Phys. Lett.*, 1996, **254**, 372–378.
- 48 P. J. F. Harris, *Philos. Mag.*, 2004, **84**, 3159–3167.
- 49 F. Ben Romdhane, J. A. Rodríguez-Manzo, A. Andrieux-Ledier, F. Fossard, A. Hallal, L. Magaud, J. Coraux, A. Loiseau and F. Banhart, *Nanoscale*, 2016, **8**, 2561–2567.
- 50 J. Goma and M. Oberlin, *Thin Solid Films*, 1980, **65**, 221–232.
- 51 J. N. Rouzaud and A. Oberlin, *Carbon*, 1989, **27**, 517–529.
- 52 B. Westenfelder, J. C. Meyer, J. Biskupek, S. Kurasch, F. Scholz, C. E. Krill and U. Kaiser, *Nano Lett.*, 2011, **11**, 5123–5127.
- 53 A. Chuvilin, U. Kaiser, E. Bichoutskaia, N. a. Besley and A. N. Khlobystov, *Nat. Chem.*, 2010, **2**, 450–453.
- 54 W. Neng, L. Shuang-ying, X. Jun, M. Matteo, Z. Yi-long, W. Shu, S. Li-tao and H. Qing-an, *Nanoscale*, 2014, **6**, 11213–11218.